

Quantitative Evaluation for Skill Controller Based on Comparison With Human Demonstration

Kazuaki Hirana, Takeshi Nozaki, Tatsuya Suzuki, Shigeru Okuma, Kaiji Itabashi, and Fumiharu Fujiwara

Abstract—One of the promising strategies to design a skill controller for robots is to observe the human worker's skill and embed it in the robot controller under certain control architecture. However, no systematic design strategies to realize this scenario have yet been developed due to the lack of a quantitative performance evaluation of the skill controller. In this brief, the switching-impedance controller is considered as the skill controller and is developed based on a comparison with human worker's demonstration. The enabling condition to switch the impedance parameter is optimized by calculating a hidden Markov model (HMM) distance which can measure the similarity between the skill of the human worker and the robot. HMM is a doubly stochastic system and is recognized as a useful tool for speech recognition. Thanks to the similarity in the stochastic characteristics between speech and skill (position/force) data, HMM is also expected to play a crucial role in skill controller design. An insertion task of deformable objects with the assistance of a vision sensor is considered in this brief. Some parameters which appear in the skill controller are optimized so as to increase the similarity with human worker's demonstration.

Index Terms—Deformable object, hidden Markov model (HMM) distance, human skill, switching impedance.

I. INTRODUCTION

RECENTLY, many control strategies for assembly tasks have been proposed [7]–[15]. In [9]–[11], the manipulation of deformable objects has been realized in spite of the difficulty of dealing with their flexibility. However, in the case of handling deformable objects, since a complete physical model of the assembly task cannot be simply made and the appropriate control parameters cannot be easily specified, the designer is obliged to go through a painful trial and error procedure in order to determine a reasonable control structure and parameters.

In contrast, human workers seem to be able to accomplish complex assembly tasks smoothly. From this observation, several studies have been carried out focusing on the transfer of human skill to the robot controller [9], [12]. The common strategy used in these studies was to observe the worker's data and to embed it in the robot controller using a certain control architecture. Although these approaches enable the robot to imitate human workers, the robot may not be able to adapt to a small change in the environment and/or an unexpected disturbance during a playback mode since the obtained human worker's data are generally stored as time-series data.

Generally speaking, the important aspects of the human worker's operation can be described as follows: 1) human workers control the motion of their fingertips based on the interactive force with the environment and on their position relative to it; 2) human workers change the dynamics (impedance) according to the contact configuration during the assembly task; and 3) human workers make use of visual information in order to accomplish a task which involves handling deformable objects. From these points of view, it seems natural to realize a skill controller based on "switching impedance control" and "supervisor," which switches the impedance parameters according to the contact configuration during the assembly process. This leads to a so-called hybrid system framework that is attracting great attention in the system control field [15]. In case of considering the assembly task, however, it is very difficult to develop a systematic design procedure due to the lack of a quantitative performance evaluation of the skill.

The hidden Markov model (HMM) [2] is capable of characterizing a doubly stochastic process with an underlying immeasurable stochastic process and an observable stochastic process, and is recognized as a useful tool for speech recognition. Thanks to the similarity in stochastic characteristics between speech and skill (position/force) data, the HMM is also expected to play a crucial role in the quantitative performance evaluation of the skill controller. From this point of view, the HMM has been introduced to measure the similarity of assembly skill [14] and HMM distance has been introduced to identify human driving skill [6]. These works, however, have not introduced any control oriented ideas and have not regarded the HMM as a tool to optimize control parameters.

In this brief, a design methodology for a skill controller based on a comparison with human demonstration is proposed. An insertion task of the deformable hose is considered throughout this brief. The switching impedance controller is adopted as a basic control architecture. In this framework, a set of impedance parameters and enabling conditions (event observer) to facilitate impedance switching must be designed. The impedance parameters are directly identified from the human worker's data. The enabling conditions, however, cannot be acquired by simply observing the profile of the human worker's data. In order to determine the enabling conditions, the HMM distance is used to measure the similarity of skills between the human worker and the robot in which specified enabling conditions are implemented. Based on the measured similarity, the semioptimal enabling conditions (in the sense that the robot skill resembles the skill demonstrated by the human worker) are found after several trials.

This brief is organized as follows. In Section II, a HMM framework is reviewed. The architecture of the proposed hybrid

Manuscript received September 6, 2002; revised August 26, 2003. Manuscript received in final form October 20, 2003. Recommended by Associate Editor M. Lemmon.

The authors are with Department of Electrical Engineering, Nagoya University, Nagoya 464-8603, Japan (e-mail: hirana@okuma.nuee.nagoya-u.ac.jp).

Digital Object Identifier 10.1109/TCST.2004.824955

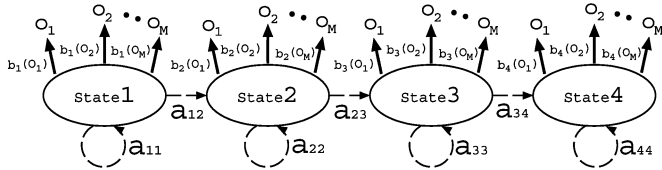


Fig. 1. Left-to-right HMM.

controller and its evaluation strategy are discussed in Section III. Finally, the proposed design method is applied to a hose insertion task in Section IV.

II. HMM

In this section, a brief review of the HMM [2] is described.

A. Mathematical Definition of HMM

The standard HMM is a collection of finite states connected by transitions and is characterized by the following three parameters:

- 1) the state-transition probability distribution from state i to j : $A = \{a_{ij}\}$;
- 2) the occurrence probability distribution of observation symbol o_k at state j : $B = \{b_j(o_k)\}$; and
- 3) the initial state-probability distribution: $\Pi = \{\pi_i\}$.

If the numbers of states and observation symbols are denoted by N and T , respectively, then $1 \leq i \leq N, 1 \leq j \leq N$, and $1 \leq k \leq T$ must hold. For convenience, the notation $\lambda = (A, B, \Pi)$ is used to specify the HMM. As an example, a left-to-right model with four states is depicted in Fig. 1.

B. Vector Quantization as Preprocessing

In order to apply some mathematical algorithms provided for the HMM to a particular situation, the observed physical signals must be transformed to symbols by compressing the original data to lower dimensional data. In this brief, a self organizing map (SOM) developed by Kohonen [4] is used as a vector quantization tool.

SOM is a kind of unsupervised vector-quantization algorithm. It projects the observed limited dimensional data vector onto the lower dimensional space while maintaining the phase relationship between each data. The quantization is carried out so as to minimize the sum of the distances between the reference vector and the data vector. See [4] for details.

Another vector-quantization algorithm, such as the competitive and selective learning (CSL) algorithm [5], can be an alternative candidate for the preprocessing. In our preliminary experiments, however, the likelihood of an HMM with a CSL algorithm was smaller than that of an HMM with a SOM. Therefore, we have decided to adopt the SOM as the preprocessing algorithm for the HMM.

C. Useful Algorithms for HMM

The following two basic problems have been addressed in the HMM.

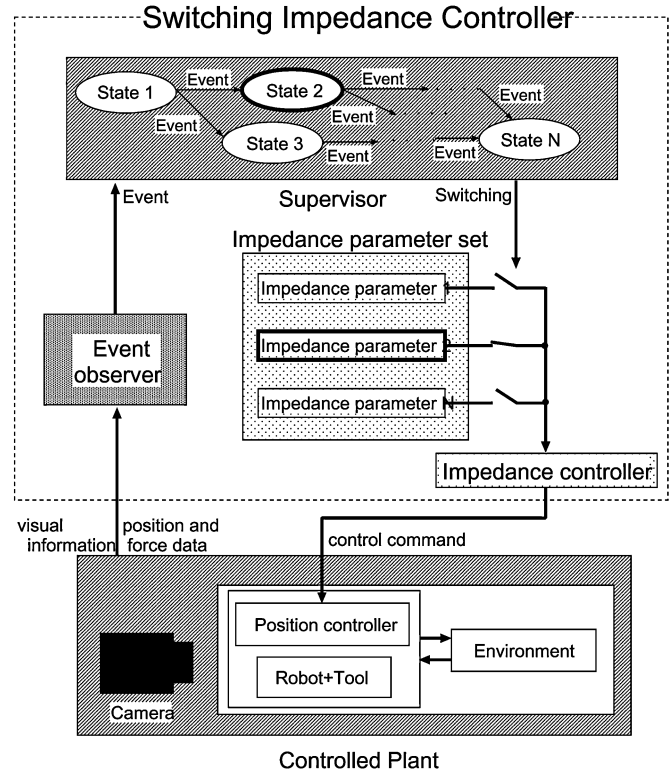


Fig. 2. Skill controller for assembly tasks based on switching impedance controller.

- 1) How to compute $P(O | \lambda)$ when the occurrence probability of the output symbol sequence $O = o_1 o_2 \dots o_T$ when the model λ is given.
- 2) How to estimate the parameters of HMM λ when the output sequence O is given.

As for problem (1), it is well known that the computational time increases exponentially with the increase of the length of the output symbol sequence. To overcome this problem, a forward algorithm has been developed. Equation (2) means an identification of the HMM, in other words, the problem to find the most possible HMM when the output symbol sequence is observed. The Baum–Welch algorithm, which includes the forward algorithm, is known as a useful algorithm to solve this problem. Note that the obtained model λ is not always global optimal because the Baum–Welch algorithm is inherently a kind of steepest descent method. See [2] for details.

D. Distance Between Two HMMs

The distance between two HMMs has been defined in [3], which can measure the similarity between two stochastic models in a quantitative manner. The distance D_s between HMMs λ_i and λ_j is defined as follows:

$$D_s(\lambda_i, \lambda_j) = \frac{D(\lambda_i, \lambda_j) + D(\lambda_j, \lambda_i)}{2} \quad (1)$$

where

$$D(\lambda_i, \lambda_j) = \frac{1}{T_j} \{\log P(O_j | \lambda_j) - \log P(O_j | \lambda_i)\}. \quad (2)$$

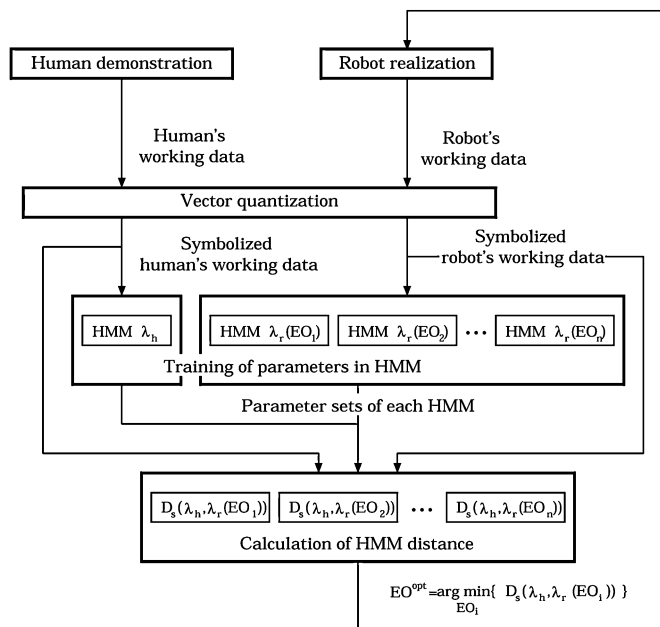


Fig. 3. Process of optimization of event observer.

O_j denotes the observed symbol sequence, and T_j denotes the length of O_j . Since $D(\lambda_i, \lambda_j)$ is not generally symmetric, i.e.,

$$D(\lambda_j, \lambda_i) = \frac{1}{T_i} \{ \log P(O_i | \lambda_i) - \log P(O_i | \lambda_j) \} \\ \neq D(\lambda_i, \lambda_j)$$

the average of the two nonsymmetric distances is adopted. The distance D_s can be interpreted as a variation of the Kullback–Liebler divergence developed in information theory [3]. D_s can be computed by using the forward algorithm mentioned above.

III. PROPOSED FRAMEWORK OF SKILL CONTROLLER DESIGN FOR ASSEMBLY TASKS

A. Architecture of Skill Controller for Assembly Tasks

In order to realize a skill similar to that of a human worker, a skill controller based on the switching impedance controller is considered (Fig. 2).

The plant is a continuous system which consists of a robot, a tool, a position controller, an environment, and a camera. Outputs of the plant are a position of the endpoint of the manipulator, a force exerted to it, and a configuration of the tool measured by the CCD camera. The event observer detects the change of the contact state (contact configuration) of the plant by observing outputs of the plant, and sends the event information to the supervisor. The supervisor is realized by a finite automaton in which each state corresponds to each state of the task and causes the switching of impedance parameters. The enabling condition for the switching of the state in the supervisor is specified by the occurrence of events detected by the event observer. The impedance controller tries to realize the impedance specified by the supervisor by sending the position command to

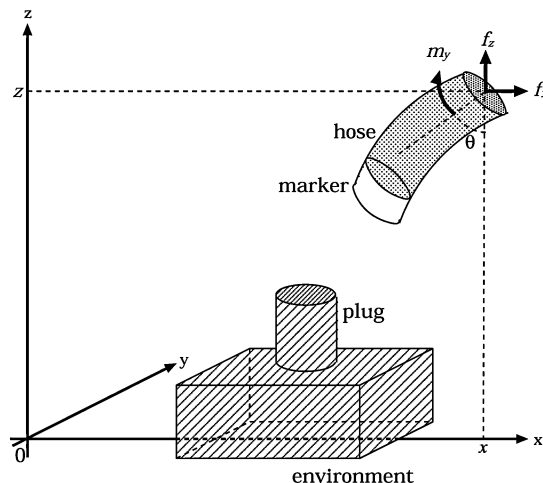


Fig. 4. Hose insertion task.

the “position controller.” As a result, the motion of the robot is characterized by the set of enabling conditions (events) and impedance parameters which vary according to the contact configuration.

1) *Acquisition of Data Demonstrated by Human Worker:* Our controller design strategy is based on a profile of data demonstrated by human workers. The profile may include the position of the endpoint of the manipulator, the interactive force between the manipulator and the environment, and some feature values for the configuration of the tool. The human demonstration is carried out under a “pseudo environment” which can reflect the “real environment.”

2) *Identification of Human’s Working Impedance:* In the next step, the profile of the impedance parameters used by the human worker is identified based on the human’s measured working data profile. The impedance model should have following dynamics. (See Fig. 17).

$$C_x(\dot{x} - \dot{x}_d) + K_x(x - x_d) = f_x - f_{xd} \quad (3)$$

$$C_z(\dot{z} - \dot{z}_d) + K_z(z - z_d) = f_z - f_{zd} \quad (4)$$

$$C_\theta(\dot{\theta} - \dot{\theta}_d) + K_\theta(\theta - \theta_d) = m_y - m_{yd}. \quad (5)$$

Throughout this brief, the motion of the object should be restricted in the two-dimensional plane (specified by x and z). x, z and θ represent the positions and rotation on each coordinate. Also, f_x, f_z and m_y represent the forces and the moment on each coordinate. These data are acquired from human demonstration as described in the previous subsection. The parameters $C_{x,z,\theta}$ and $K_{x,z,\theta}$ are impedance parameters of so-called “damping” and “spring,” respectively. The subscripts x, z and θ indicate the coordinates. The variables x_d, z_d, θ_d and f_{xd}, f_{zd}, m_{yd} denote the “reference positions” and the “reference forces,” respectively. These reference signals should be constant throughout the task. Impedance parameters are identified by applying a recursive weighted least square (WLS) algorithm with a forgetting factor. In the following, the identification process is briefly described focusing on the x direction [i.e., (3)].

First of all, (3) is transformed to its transfer function form in the manner of (6) with the addition of a low-pass filter in order to avoid taking direct derivatives

$$\begin{aligned} X(s) &= \frac{1}{C_x s + K_x} F_x(s) \\ &= \frac{\left\{ \frac{1}{\tau s + 1} \right\}}{\left\{ \frac{C_x s + K_x}{\tau s + 1} \right\}} F_x(s) \end{aligned} \quad (6)$$

where

$$\begin{aligned} X(s) &= \mathcal{L}[x(t) - x_d(t)] \\ F_x(s) &= \mathcal{L}[f_x(t) - f_{xd}(t)] \end{aligned}$$

and $\mathcal{L}[\cdot]$ denotes a Laplace transformation. By letting $s = (2/T)(1 - z^{-1}/1 + z^{-1})$, the following can be derived:

$$C_x(k)X_0(k) + K_x(k)X_1(k) = F_1(k) \quad (7)$$

where

$$\begin{aligned} X_0(k) &= \frac{2(1 - z^{-1})}{2\tau(1 - z^{-1}) + T(1 + z^{-1})} X(k) \\ X_1(k) &= \frac{T(1 + z^{-1})}{2\tau(1 - z^{-1}) + T(1 + z^{-1})} X(k) \\ F_1(k) &= \frac{T(1 + z^{-1})}{2\tau(1 - z^{-1}) + T(1 + z^{-1})} F(k) \\ X(k) &= \mathcal{Z}[x(k) - x_d(k)] \\ F(k) &= \mathcal{Z}[f_x(k) - f_{xd}(k)] \end{aligned}$$

and $\mathcal{Z}[\cdot]$ denotes a z-transformation.

In the recursive WLS identification algorithm, the polynomials $A(z^{-1})$ and $B(z^{-1})$ are updated so as to minimize the WLS error of w in the following model:

$$y(k) = \frac{B(z^{-1})}{A(z^{-1})} u(k) + w(k) \quad (8)$$

where

$$\begin{aligned} A(z^{-1}) &= 1 + a_1 z^{-1} + \dots + a_n z^{-n}, \\ B(z^{-1}) &= b_0 z^{-1} + b_1 z^{-1} + \dots + b_n z^{-n}. \end{aligned}$$

By introducing following variables:

$$\begin{aligned} \alpha(k) &= [-a_1 \quad -a_2 \quad \dots \quad -a_n \quad b_0 \quad b_1 \quad \dots \quad b_n]^T \\ \Omega(k) &= [y(k-1) \quad y(k-2) \quad \dots \quad y(k-n) \\ &\quad u(k-1) \quad u(k-2) \quad \dots \quad u(k-n)]^T. \end{aligned}$$

Equation (8) can be rewritten as follows:

$$y(k) = \Omega(k)^T \alpha(k) + w(k). \quad (9)$$

Then, the estimated parameter $\hat{\alpha}(k)$ is updated by following algorithms:

$$\begin{aligned} \hat{\alpha}(k+1) &= \hat{\alpha}(k) + P(k+1)\Omega(k+1)\{y(k+1) \\ &\quad - \Omega^T(k)\hat{\alpha}(k)\} \end{aligned} \quad (10)$$

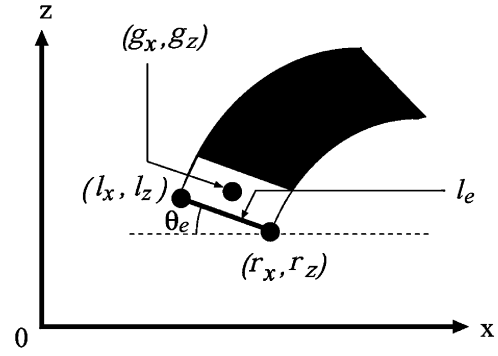


Fig. 5. Feature values of the marker.

$$\begin{aligned} P(k+1) &= \frac{1}{\lambda} \left\{ P(k) \right. \\ &\quad \left. - \frac{P(k)\Omega(k+1)\Omega^T(k+1)P(k)}{\lambda + \Omega^T(k+1)P(k)\Omega(k+1)} \right\} \end{aligned} \quad (11)$$

where λ is “forgetting coefficient.”

In order to apply this recursive WLS algorithm to the identification of C and K , it is sufficient to let

$$\begin{aligned} \alpha(k) &= \left[-\frac{K_x(k)}{C_x(k)} \quad \frac{1}{C_x(k)} \right]^T \\ \Omega(k) &= [X_1(k) \quad F_1(k)]^T \\ y(k) &= X_0(k). \end{aligned}$$

3) *Calculation of Target Impedance:* As a final step of preprocessing in designing the skill controller, the human’s working data profile is manually divided into time slots by referring to the discrete transitions of the contact configurations. The number of time slots is equal to the number of states which appear in a state transition path. The “impedance parameter set” shown in Fig. 2 is determined by taking the average value of the identified impedance parameters in each time slot. The calculated impedance parameter is called “target impedance.”

Note that the manual segmentation described above can be rough. This segmentation is made only to estimate the average impedance in each contact configuration (i.e., the impedance parameter set in Fig. 2), and is not intended to specify the switching time in the proposed controller architecture. The switching of the impedance parameter is caused by the event observer.

4) *Design of Event Observer:* A role of event observer is to determine whether the current discrete state in the controlled plant is able to switch to the next state by comparing the plant outputs with the prespecified threshold values. It is natural to pay attention to the system output which shows the largest change during the state transition. Therefore, the design problem of the event observer can be recast as the determination of the threshold value of the output variable which shows the largest change during the state transition.

5) *Evaluation and Optimization of Event Observer:* The number of states and the target impedance can be easily determined by observing the human demonstration. The threshold values specified in the event observer, however, are not as easy to detect as other parameters since they underlie the human’s working data profile. In this brief, we try to find the “good”

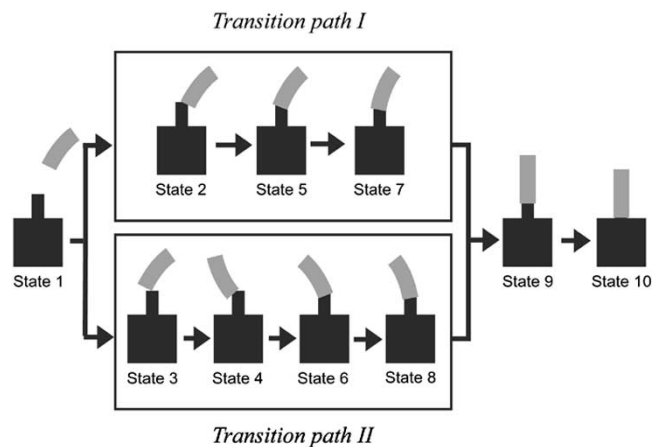


Fig. 6. Definition of state transition paths of hose insertion task.

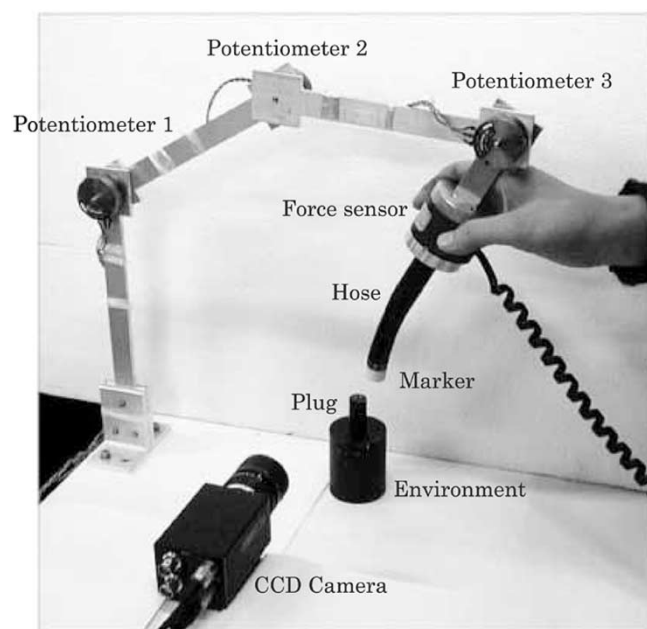


Fig. 7. A pseudoenvironment to acquire human's working data.

threshold values used in the event observer by referring to the similarity between the performance of the robot and that of the human worker as measured by the HMM distance.

Supposing that there exist s discrete states, the event observer (EO) is parameterized as follows:

$$EO = (q_1, \dots, q_{s-1}) \quad (12)$$

where $q_i (i = 1, \dots, s - 1)$ denotes the threshold value which enables the supervisor to switch the state from i to $i + 1$. q_i must be specified for one of the output variables, i.e., the position signal, the force signal, or the feature value of the tool acquired by CCD camera. Thus, the design of the event observer can be formulated as the optimization problem of these parameters, and expressed by

$$\text{Find EO which minimizes } D_s(\lambda_h, \lambda_r(EO)) \quad (13)$$

where λ_h and $\lambda_r(EO)$ represent the HMM whose construction is based on the profile of human's working data and the robot's

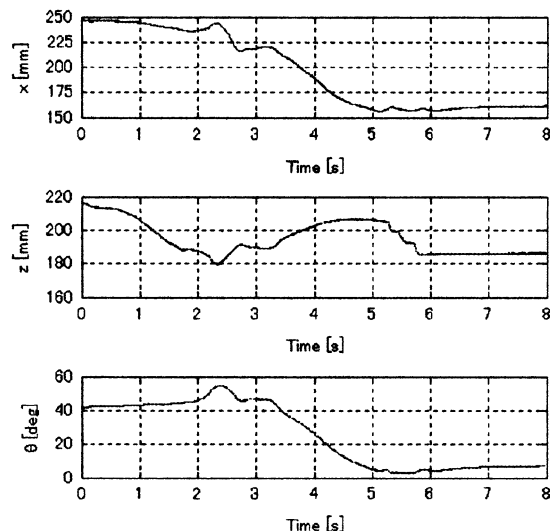


Fig. 8. Position profile of human worker 1 (Transition path I).

working data in which the EO is implemented, respectively. D_s denotes the distance between λ_h and $\lambda_r(EO)$ as formulated in (1). Note that the number of states in the HMM is not necessarily the same as the number of discrete states, i.e., contact configurations.

The optimization process of the event observer is shown in Fig. 3. From the viewpoint of optimization, it is natural that all parameters included in the EO are searched simultaneously. However, since this kind of simultaneous optimization usually requires an unreasonably large amount of computations, these parameters are optimized step by step (from q_1 to q_{s-1}) in our optimization process.

IV. APPLICATION TO HOSE INSERTION TASK

In this section, the proposed framework is applied to a hose insertion task, which includes the handling of a deformable tool. A hose insertion task is illustrated in Fig. 4. The following constraints are imposed on the hose insertion task.

- The motion of the hose is restricted in the $x - z$ plane.
- The position of the endpoint of the manipulator is expressed by (x, z) and the angle between the tool and the z axis is denoted by θ .
- The force exerted to the endpoint of the manipulator is expressed by f_x (force along x axis), f_z (force along z axis), and m_y (moment around y axis).
- A white marker is attached to the tip of the hose, and the feature values of the marker are defined by the following parameters: the position of the centroid (g_x, g_z), the position of the left down vertex (l_x, l_z), the position of the right down vertex (r_x, r_z), the distance l_e between the left down vertex and the right down vertex, and the angle θ_e between the bottom edge of the hose and x axis (see Fig. 5). These feature values are measured by the CCD camera fixed on the environment.

A. Acquisition of Human's Working Data

A pseudoenvironment to acquire the human's working data has been developed as shown in Fig. 7. It consists of a 3 degree

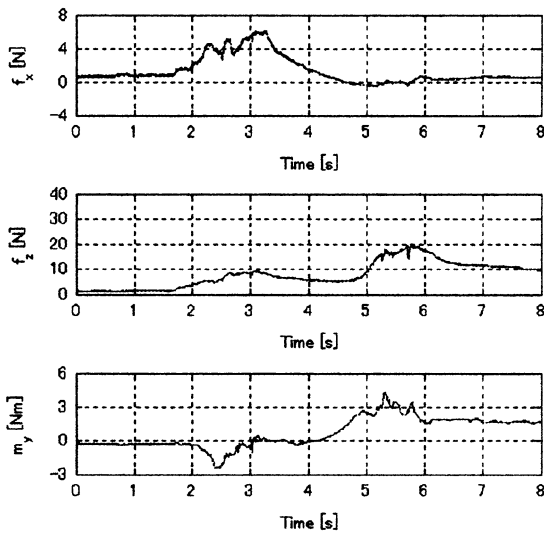


Fig. 9. Force profile of human worker 1 (Transition path I).

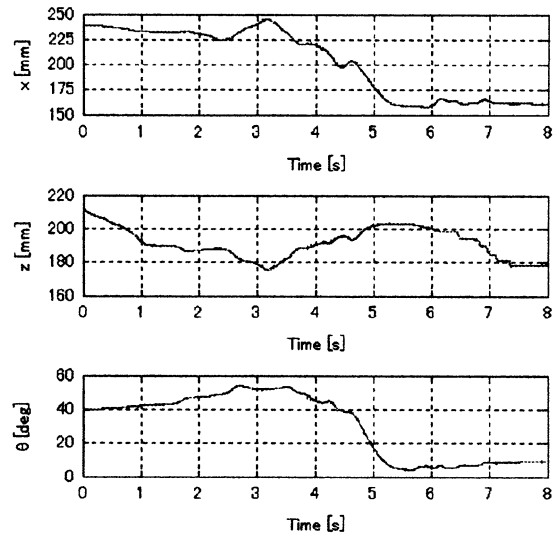


Fig. 11. Position profile of human worker 2 (Transition path I).

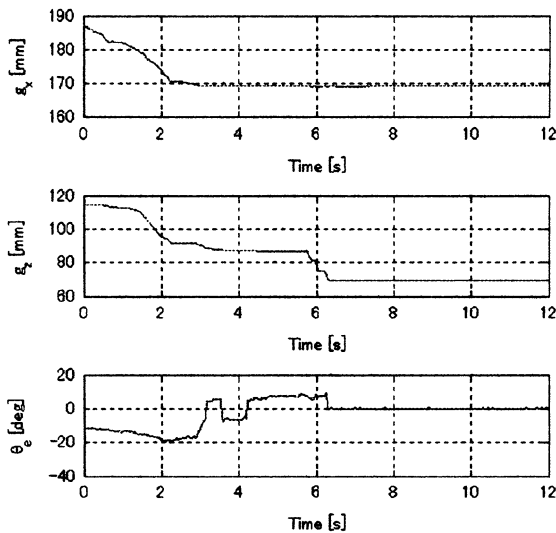


Fig. 10. Feature value profile of human worker 1 (Transition path I).

of freedom (d.o.f.) planar arm with three potentiometers, a force sensor, a hose, a CCD camera, and an environment. The force sensor is fixed to the tip of the tool. The camera is used to acquire information regarding the deformation of the hose. Human workers do not feel any incongruity throughout the execution of the task.

In the hose insertion task, the state transitions of the contact configurations are determined as shown in Fig. 6. Generally speaking, there are a considerable number of ways for the discrete transitions to occur in the handling of a deformable object. It is, however, undesirable to define obviously meaningless transitions from the viewpoint of controller design. Therefore, we have restricted our discussion to two paths that were obtained through the observation of the human demonstration. Three humans' working data along transition path I are shown in Figs. 8–16.

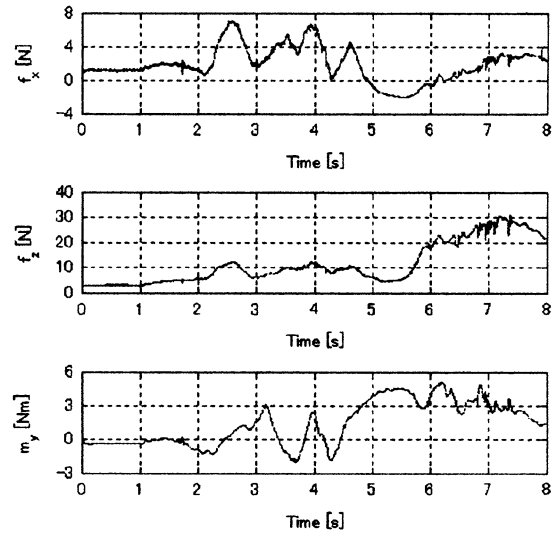


Fig. 12. Force profile of human worker 2 (Transition path I).

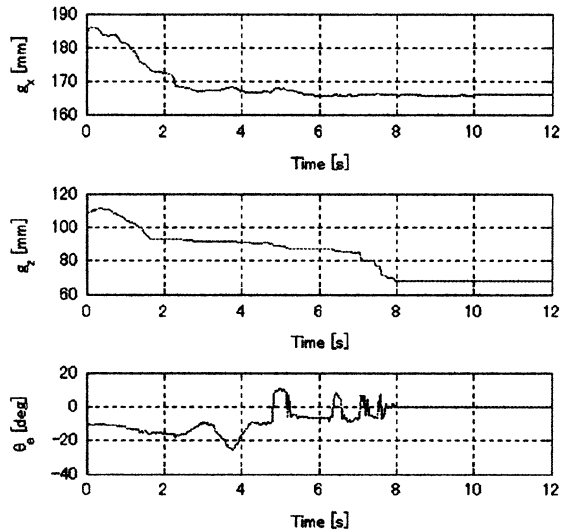


Fig. 13. Feature value profile of human worker 2 (Transition path I).

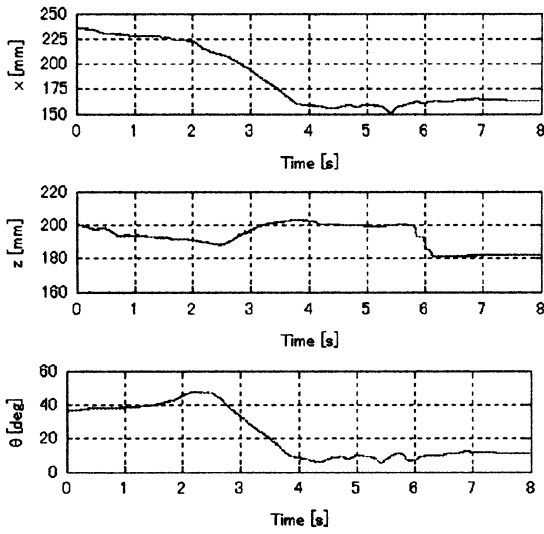


Fig. 14. Position profile of human worker 3 (Transition path I).

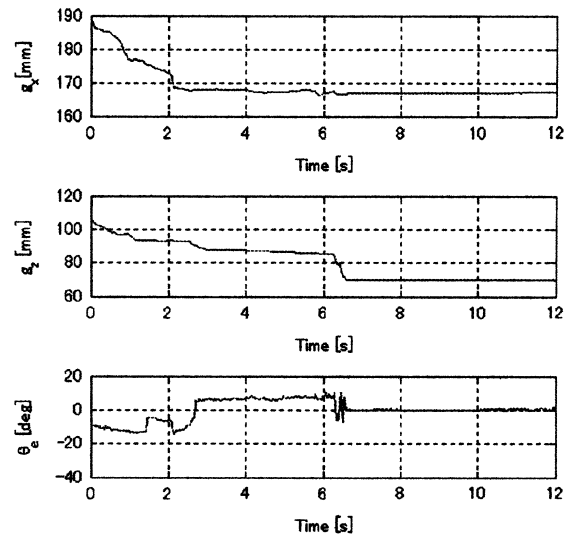


Fig. 16. Feature value profile of human worker 3 (Transition path I).

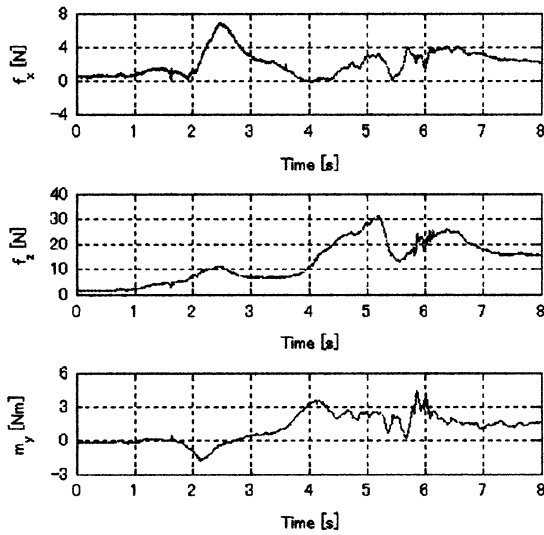


Fig. 15. Force profile of human worker 3 (Transition path I).

B. Extraction of Control Parameters From Human's Working Data

In order to develop the skill controller for the hose insertion task, the control parameters underlying human's working data, such as the set of impedance parameters and threshold values in the event observer, are extracted.

The impedance model of the hose insertion task is illustrated in Fig. 17. The identified impedance profile along the z axis used by worker 1 is shown in Fig. 18. The division of the working data of worker 1 was made as depicted in Fig. 19. As mentioned in Section III-A-3, this segmentation can be rough. As a result, the target impedance at each state was calculated by taking an average of three workers' target impedances of each state as shown in Fig. 20.

Next, the event observer was parameterized by using the following output variables acquired from the observation of human demonstration.

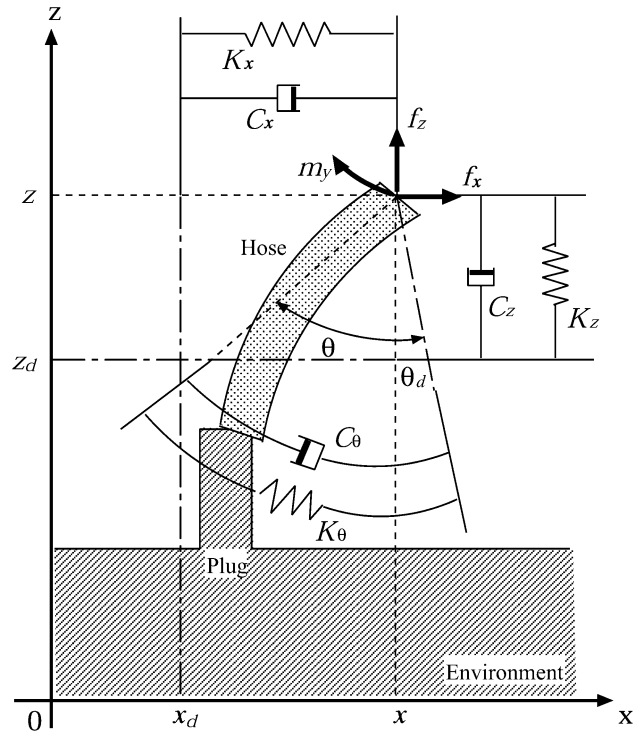


Fig. 17. Impedance model of hose insertion task.

Transition path I:

- Transition from state 1 to 2:
Force along z axis ($f_z \geq f_{z_{th1}}$).
- Transition from state 2 to 5:
Position of the right down vertex of the marker ($r_x \leq r_{x_{th1}}$).
- Transition from state 5 to 7:
Angle between the bottom of the marker and x axis ($\theta_e \geq \theta_{e_{th1}}$).
- Transition from state 7 to 9:
Angle of the hose around y axis ($\theta \leq \theta_{th1}$).

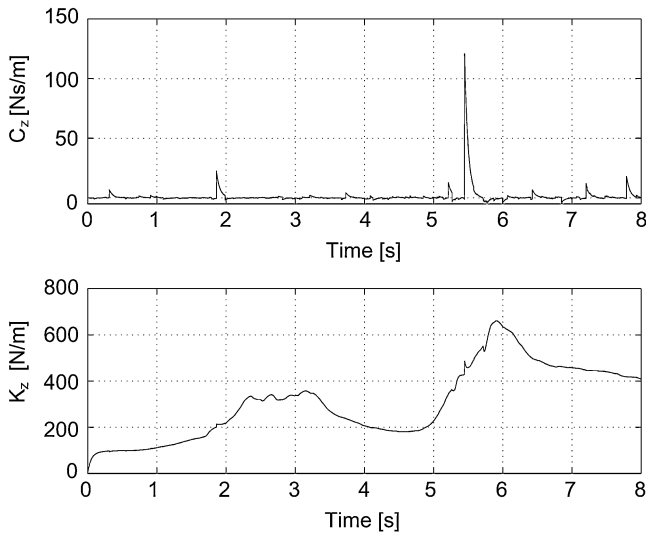


Fig. 18. Identified human's working impedance of worker 1 (z axis) (Transition path I).

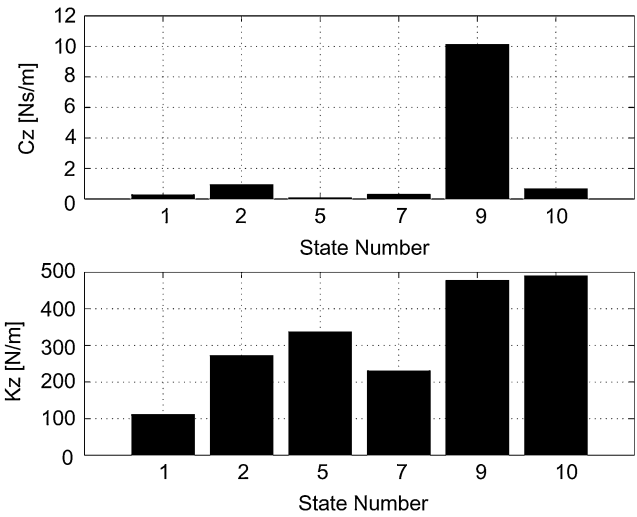


Fig. 20. Calculated target impedance of each state (z axis) (Transition path I).

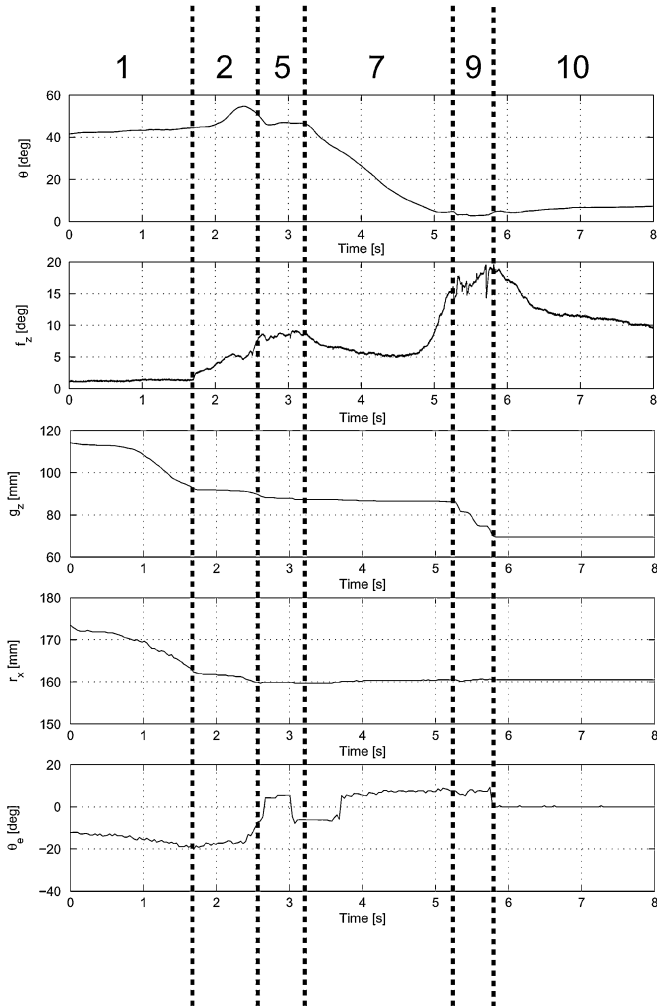


Fig. 19. Division of human's working data profile of worker 1 (Transition path I).

- Transition from state 9 to 10:
Position of the centroid of the marker in z axis ($g_z \leq g_{z_{th1}}$).

Transition path II:

- Transition from state 1 to 3:
Force along z axis ($f_z \geq f_{z_{th2}}$).
- Transition from state 3 to 4:
Angle of the hose around y axis ($\theta \leq \theta_{1_{th2}}$).
- Transition from state 4 to 6:
Position of the left down vertex of the marker ($l_x \geq l_{x_{th2}}$).
- Transition from state 6 to 8:
Angle between the bottom of the marker and x axis ($\theta_e \leq \theta_{e_{th2}}$).
- Transition from state 7 to 9:
Angle of the hose around y axis ($\theta \geq \theta_{2_{th2}}$).
- Transition from state 9 to 10:
Position of the centroid of the marker in z axis ($g_z \leq g_{z_{th2}}$).

Now, the optimization problem can be formulated as follows:

Transition path I:

Find $(f_{z_{th1}}, r_{x_{th1}}, \theta_{e_{th1}}, \theta_{th1}, g_{z_{th1}})$
which minimizes $D_s(\lambda_h, \lambda_r)$. (14)

Transition path II

Find $(f_{z_{th2}}, \theta_{1_{th2}}, l_{x_{th2}}, \theta_{e_{th2}}, \theta_{2_{th2}}, g_{z_{th2}})$
which minimizes $D_s(\lambda_h, \lambda_r)$. (15)

Note that some feature values of hose (r_x, θ_e, l_x, g_z) are included in order to detect the deformation of the hose. This implies that visual information plays an essential role in the hose insertion task.

In order to optimize the event observer, some experiments and evaluations were carried out alternately. The experimental setup for the hose insertion task is illustrated in Fig. 21. A position control-based manipulator, PA-10, was used for this experiment. In order to detect the deformation of the hose, a camera was

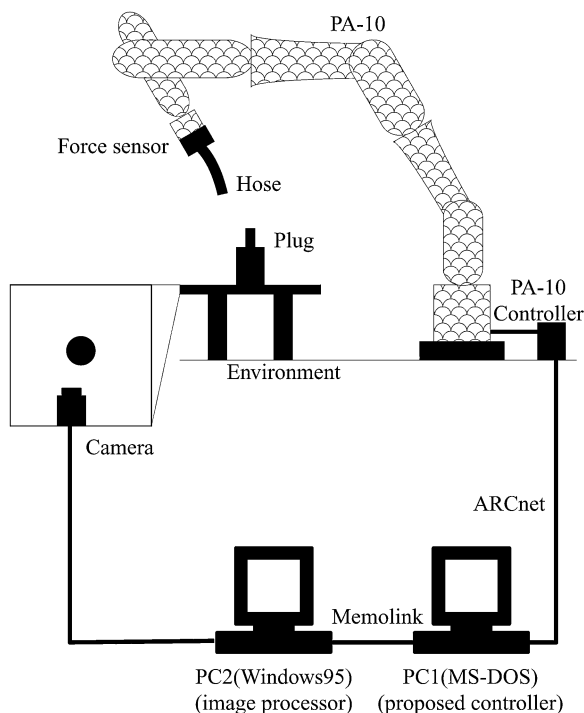


Fig. 21. Experimental setup for hose insertion task.

fixed on the work table. The image information obtained by the camera is transferred to PC2. In PC2, a hardware image processor (MVC150/40) is installed and the necessary image processing is carried out in real-time. This processor outputs the feature values of the marker attached to the hose every 66 [ms], and transfers them to PC1 via a dual port memory (MEMOLINK). The proposed controller was implemented on PC1, and PC1 outputs the position command to PA-10 every 10 [ms].

C. Representation of Working Data by HMM

The similarity between the human's working data and the robot's is measured by the HMM distance. In order to calculate the HMM distance, each working data must be modeled using HMM.

First of all, the working data must be symbolized (quantized). In our case, the working data consists of the position (x, z, θ) , the force (f_x, f_z, m_y) and the feature value of the hose (g_x, g_z, θ_e) . These data are quantized and transformed into symbol sequences by applying SOM. The training data for the SOM consists of three human's working data and the robot's working data obtained by testing various event observers EO_i . All of working data are quantized based on the common set of symbols.

The next step involves determining the structure of the HMM. For simplicity, the left-to-right HMM was chosen and the number of states has been determined so as to maximize the likelihood value for the data of worker 1. The Baum-Welch algorithm has been used to calculate the maximum likelihood value for each state number. Tables I and II show the variation of the likelihood value for the number of states. From these two tables, the optimal number of states for the transition path I can be concluded as five, and the one for transition path II can be concluded as six, respectively. Note that neither of them

TABLE I
RELATION BETWEEN LIKELIHOOD AND NUMBER OF STATES (TRANSITION I)

state	$\log P(O \lambda)$
3	-3571
4	-3138
5	-2816
6	-2684
7	-2501

TABLE II
RELATION BETWEEN LIKELIHOOD AND NUMBER OF STATES (TRANSITION II)

state	$\log P(O \lambda)$
3	-3683
4	-3333
5	-3025
6	-2757
7	-2725

TABLE III
EVALUATION VALUES OF $f_{z_{th1}}$

$f_{z_{th1}}[N]$	D_s	$f_{z_{th1}}[N]$	D_s
1.1	51.94	1.6	47.48
1.2	50.07	1.7	47.91
1.3	48.68	1.8	47.08
1.4	47.69	1.9	47.21
1.5	48.84	2.0	49.09

coincide with the number of physical contact configurations included in each transition path. This implies that the state of HMM no longer coincides with that of the physical state.

Finally, the HMM λ_h of human's working data and the HMM $\lambda_r(EO_i)$ of robot's working data were constructed by applying the Baum-Welch algorithm to the quantized (symbolized) working data. Here, the human HMM λ_h has been decided in the following way. First, three human HMMs were constructed by applying the Baum-Welch algorithm to the symbol sequences of three human workers independently. Then, one HMM, which has shown the highest likelihood value, has been selected as the λ_h .

D. Optimization Results

Based on λ_h and $\lambda_r(EO_i)$ calculated in the previous subsection, EO_i is optimized so as to minimize the HMM distance $D_s(\lambda_h, \lambda_r(EO_i))$. As mentioned in Section III.A.5, the parameters of EO have been optimized step by step as follows in order to avoid a combinatorial explosion:

As for transition path I

$$\begin{aligned}
 \text{Initial setting : } EO^{\text{init}} &= (f_{z_{th1}}^{\text{init}}, r_{x_{th1}}^{\text{init}}, \theta_{e_{th1}}^{\text{init}}, \theta_{th1}^{\text{init}}, g_{z_{th1}}^{\text{init}}) \\
 \text{1st optimization : } EO^{\text{opt1}} &= (f_{z_{th1}}^{\text{opt1}}, r_{x_{th1}}^{\text{opt1}}, \theta_{e_{th1}}^{\text{opt1}}, \theta_{th1}^{\text{opt1}}, g_{z_{th1}}^{\text{opt1}}) \\
 \text{2nd optimization : } EO^{\text{opt2}} &= (f_{z_{th1}}^{\text{opt2}}, r_{x_{th1}}^{\text{opt2}}, \theta_{e_{th1}}^{\text{opt2}}, \theta_{th1}^{\text{opt2}}, g_{z_{th1}}^{\text{opt2}}) \\
 &\vdots \\
 \text{Final optimization : } EO^{\text{opt}} &= (f_{z_{th1}}^{\text{opt}}, r_{x_{th1}}^{\text{opt}}, \theta_{e_{th1}}^{\text{opt}}, \theta_{th1}^{\text{opt}}, g_{z_{th1}}^{\text{opt}})
 \end{aligned}$$

As for transition path II, a similar optimization procedure was adopted. The results of optimization for each transition path are listed in Tables III to XIII. The bold font reveals the optimal result. The range of search was determined based on the feasibility of the task. We can see that all parameters have been determined

TABLE IV
EVALUATION VALUES OF $r_{x_{th1}}$

$r_{x_{th1}}$ [mm]	D_s	$r_{x_{th1}}$ [mm]	D_s
692.50	52.34	693.75	54.16
692.75	53.00	694.00	55.85
693.00	50.34	694.25	56.90
693.25	52.85	694.50	54.71
693.50	54.06	694.75	52.97

TABLE V
EVALUATION VALUES OF $\theta_{e_{th1}}$

$\theta_{e_{th1}}$ [deg]	D_s	$\theta_{e_{th1}}$ [deg]	D_s
-5.0	53.43	-7.5	52.01
-5.5	53.54	-8.0	51.87
-6.0	53.09	-8.5	51.37
-6.5	48.41	-9.0	52.24
-7.0	51.81	-9.5	52.01

TABLE VI
EVALUATION VALUES OF θ_{th1}

θ_{th1} [deg]	D_s	θ_{th1} [deg]	D_s
5.0	46.46	7.5	50.32
5.5	45.40	8.0	48.43
6.0	48.18	8.5	48.91
6.5	48.75	9.0	49.91
7.0	52.07	9.5	49.56

TABLE VII
EVALUATION VALUES OF $g_{z_{th1}}$

$g_{z_{th1}}$ [mm]	D_s	$g_{z_{th1}}$ [mm]	D_s
360.75	51.40	362.00	52.96
361.00	52.88	362.25	48.92
361.25	51.69	362.50	52.99
361.50	50.15	362.75	49.87
361.75	50.39	363.00	50.09

TABLE VIII
EVALUATION VALUES OF $f_{z_{th2}}$

$f_{z_{th2}}$ [mm]	D_s	$f_{z_{th2}}$ [mm]	D_s
0.8	59.03	1.3	53.72
0.9	60.85	1.4	55.92
1.0	58.86	1.5	58.39
1.1	59.87	1.6	60.14
1.2	59.99	1.7	60.58

TABLE IX
EVALUATION VALUES OF θ_{th21}

θ_{th21} [deg]	D_s	θ_{th21} [deg]	D_s
-2.4	55.87	-2.9	55.18
-2.5	54.33	-3.0	60.32
-2.6	54.88	-3.1	55.04
-2.7	60.27	-3.2	61.25
-2.8	59.23	-3.3	56.13

TABLE X
EVALUATION VALUES OF $l_{x_{th2}}$

$l_{x_{th2}}$ [mm]	D_s	$l_{x_{th2}}$ [mm]	D_s
707.00	57.51	708.25	58.03
707.25	55.54	708.50	56.55
707.50	58.44	708.75	59.06
707.75	60.22	709.00	60.08
708.00	57.23	709.25	56.60

TABLE XI
EVALUATION VALUES OF $\theta_{e_{th2}}$

$\theta_{e_{th2}}$ [deg]	D_s	$\theta_{e_{th2}}$ [deg]	D_s
5.0	55.85	7.5	56.81
5.5	54.35	8.0	58.44
6.0	52.48	8.5	61.69
6.5	56.65	9.0	61.08
7.0	58.90	9.5	61.17

TABLE XII
EVALUATION VALUES OF θ_{th22}

θ_{th22} [deg]	D_s	θ_{th22} [deg]	D_s
-1.2	61.38	-1.7	58.26
-1.3	59.80	-1.8	60.74
-1.4	57.69	-1.9	57.06
-1.5	59.68	-2.0	58.66
-1.6	57.93	-2.1	59.66

TABLE XIII
EVALUATION OF $g_{z_{th2}}$

$g_{z_{th2}}$ [mm]	D_s	$g_{z_{th2}}$ [mm]	D_s
360.75	59.02	362.00	56.75
361.00	56.69	362.25	57.75
361.25	57.21	362.50	54.61
361.50	54.76	362.75	55.05
361.75	54.75	363.00	58.53

uniquely by applying the proposed evaluation technique based on HMM distance.

E. Validation of Using HMM

In order to verify the usefulness of the proposed method, the robot's working data with the optimal event observer is compared with that with the nonoptimized event observer. The former is shown in Fig. 23, while the latter is shown in Fig. 24. As a reference, the human's working data is shown in Fig. 22. When we look at these profiles, we can see that the profiles of the optimized case have more similar characteristics (especially in f_z) to the profiles of the human's working data than those of the nonoptimized case. Also, for the quantitative validation, the distances of the two cases were calculated. They were given by $D_s(\lambda_h, \lambda(\text{EO}^{\text{opt}})) = 55.21$

and $D_s(\lambda_h, \lambda(\text{EO}^{\text{nonopt}})) = 61.34$. From these distances, we can verify that the profiles of the optimized case have more similar characteristics than the nonoptimized case.

As an alternative way to measure the similarity between data generated by the human worker and that by the robot, the LMS error may be utilized. The LMS error-based approach, however, is applicable only when the two data have the same time length, and similar skills do not always have the same time length in their data profiles. Moreover, the human operation is inherently stochastic even for a repetitive task. From these points of view, the LMS error-based approach is not a suitable measuring technique for skill evaluation. However, the HMM distance-based approach is applicable even in these cases because of the stochastic characteristics of the HMM.

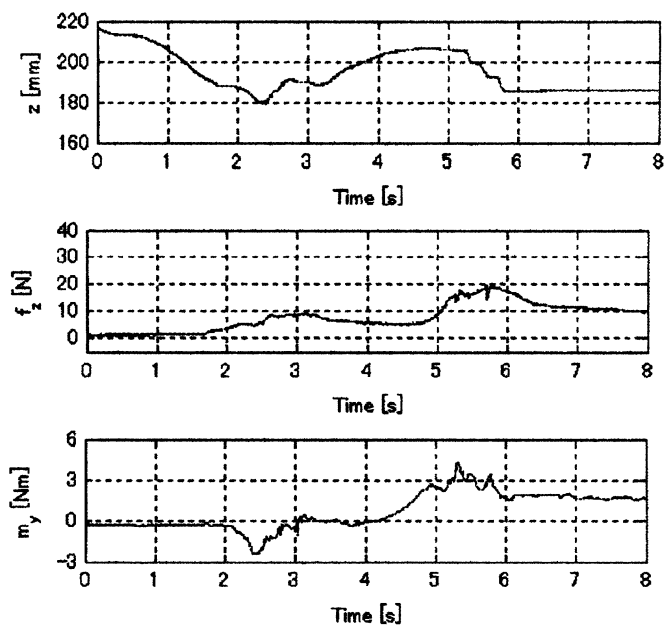


Fig. 22. Human data (Transition I).

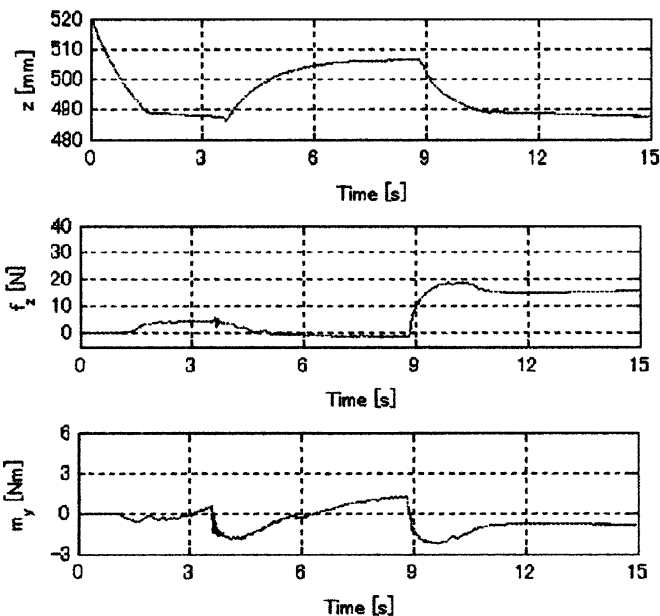


Fig. 24. Robot data with optimal event observer (Transition I).

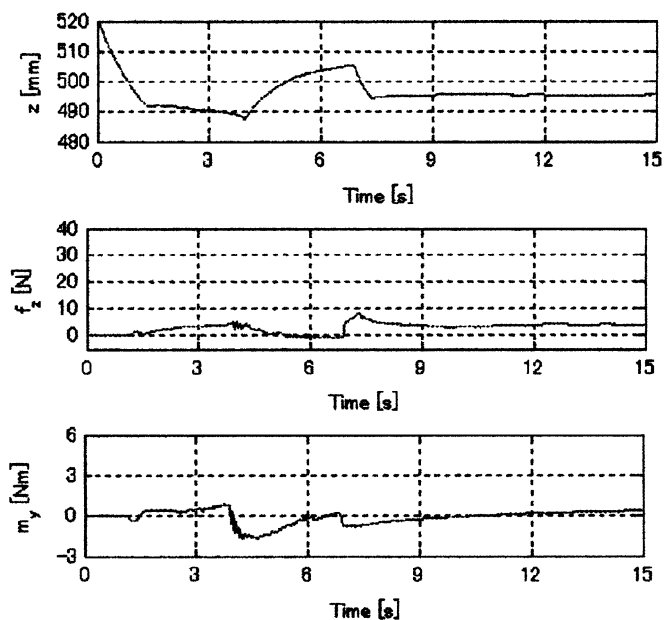


Fig. 23. Robot data with not optimal event observer (Transition I).

V. CONCLUSION

In this brief, a skill controller, which switches impedance parameters according to the task state, has been developed, and a design methodology based on a comparison with a human demonstration has been proposed. The proposed controller has been applied to a hose insertion task which involves the handling of deformable objects. In the developed control system, the event observer which detects the transition of state plays an essential role. The performance of the event observer has been evaluated by using the HMM distance between the working data demonstrated by the human worker and that generated by the robot in which the specified event observer is implemented. By introducing HMM distance, the stochastic unevenness has been

handled naturally, and the necessary parameters which appear in the event observer have been decided uniquely.

REFERENCES

- [1] N. Hogan, "Impedance control, an approach to manipulation," in *ASME J. Dynamic Syst. Measurement Control*, vol. 107-1, 1985, pp. 1-24.
- [2] L. R. Rabiner, "A tutorial on hidden markov models and selected applications in speech recognition," *Proc. IEEE*, vol. 77, pp. 257-285, Feb. 1989.
- [3] B. J. Juang and L. R. Rabiner, "A probabilistic distance measure for hidden markov models," *AT&T Tech. J.*, vol. 64, no. 2, pp. 391-408, 1985.
- [4] T. Kohonen, *Self-Organizing Map*. New York: Springer-Verlag, 1996.
- [5] N. Ueda and R. Nakano, "A new competitive learning approach based on an equidistortion principle for designing optimal vector quantizers," *Neural Netw.*, vol. 7, no. 8, pp. 1211-1227, 1994.
- [6] M. C. Nechyba and Y. Xu, "Stochastic similarity for validating human control strategy models," *IEEE Trans. Robot. Automat.*, vol. 14, pp. 437-451, June 1998.
- [7] B. Hannaford and P. Lee, "Hidden markov model analysis of force/torque information in teleoperation," *Int. J. Robot. Res.*, vol. 10, no. 5, pp. 528-539, 1991.
- [8] S. Liu and H. Asada, "Teaching and learning of deburring robots using neural networks," in *Proc. IEEE Int. Conf. Robotics and Automation*, Atlanta, GA, 1993, pp. 339-345.
- [9] S. Hirai, H. Noguchi, and K. Iwata, "Human-demonstration based approach to the recognition of process state transitions in insertion of deformable tubes," in *Proc. IEEE Int. Conf. Robotics and Automation*, MN, 1996, pp. 2006-2011.
- [10] H. Nakagaki, K. Kitagaki, T. Ogasawara, and H. Tsukune, "Study of insertion task of a flexible wire into a hole by using visual tracking observed by stereo vision," in *Proc. IEEE Int. Conf. Robotics and Automation*, 1996, pp. 3209-3214.
- [11] H. Wakamatsu, S. Hirai, and K. Iwata, "Modeling of linear objects considering bend, twist, and extensional deformations," in *Proc. IEEE Int. Conf. Robotics and Automation*, Nagoya, Japan, 1995, pp. 433-438.
- [12] Y. Tsunami, H. Naruse, D. N. Nenchev, and M. Uchiyama, "On force control in human physical skill," in *Proc. IEEE/RSJ Int. Conf. Intelligent Robots and Systems*, Grenoble, 1997, pp. 458-463.
- [13] S. Liu and H. Asada, "Transferring manipulative skills to robotics: Representation and acquisition of tool manipulative skills using a process dynamics model," in *ASME J. Dynamic Syst Measurement Control*, vol. 114, June 1992, pp. 220-228.
- [14] J. Yang, Y. Xu, and C. S. Chen, "Hidden markov model approach to skill learning and its application to telerobotics," *IEEE Trans. Robot. Automat.*, vol. 10, pp. 621-631, Oct. 1994.
- [15] B. J. McCarragher and H. Asada, "A discrete event approach to the control of robotic assembly tasks," in *Proc. IEEE Int. Conf. Robotics and Automation*, Atlanta, GA, 1993, pp. 331-336.